Development of In-situ MMC Joint Using Friction Stir Spot Welding of Al6061-T6

Neeru Chaudhary (neeru.phdmech@pec.edu.in)
Punjab Engineering College: PEC University of Technology
Sarbjit Singh
Punjab Engineering College (Deemed to be University)

Research Article

Keywords: Friction Stir Spot Welding, Silicon Carbide, Microparticles, Tensile-Shear Strength, Tool Rotation Speed, Pre-Dwelling Time

Posted Date: January 28th, 2022

DOI: https://doi.org/10.21203/rs.3.rs-1215627/v1

Abstract

In this study, friction stir spot welded joints of Al6061-T6 were obtained using Silicon Carbide particles as reinforcement. The effect of reinforced particles along with process parameters was analyzed in terms of tensile-shear strength, weld structure, hook formation. The investigations revealed that tensile-shear strength increased by 29.78 % with incorporation of silicon carbides particles in the weld region. The guiding hole diameter was found to be significant parameter for improved weld strength. Combination of moderate tool rotation speed, higher pre-dwelling time and guiding hole diameter were recognized as effective combination of process parameters. Weld cross sections were studied under stereo zoom microscope and optical microscope to observe different bonding regions. The scanning electron microscopy (SEM) and energy dispersive spectroscopy (EDS) confirmed the presence of silicon carbides particles in weld region.

1. Introduction

Nowadays, industries like aerospace and automobile etc., concentrate more on reducing weight of their machines to reduce fuel consumption, which led to increase in use of lightweight materials such as aluminium and its alloys. Initially, riveting, adhesion, resistance spot welding technique etc. were used for joining aluminium alloys [1]. However, the Friction Stir Spot Welding (FSSW) process subsequently proved to be one of the most promising means of joining aluminum and its alloys. Friction Stir Spot Welding is a solid-state welding technique which eliminates various welding defects such as growth of cracks after solidifications, thermal distortion, porosity, hot cracking, development of intermetallic compounds (IMCs) etc. [2]. The description of FSSW i.e., plunging, stirring and retracting is as shown in Fig. 1. Initially, pre-dwelling time is provided to rotating tool to soften upper surface of workpiece before start of plunging process. The rotating tool then penetrates into soften workpiece and increases temperature of workpiece, leading to thermal softening of material in stirring zone. During plunging, rotating tool performs extrusion of thermally softened material with the help of specially designed grooves on tool pin profile by transferring material from one position to another. During plunging and transferring material around tool pin, there are chances of expelling of material which has been countered by tool shoulder using forging action on weld zone. After reaching a predefined depth tool rotates in workpieces for specified dwell time, known as stirring stage. After performing desired joining operation, the rotating tool retracts from workpiece.

Different researchers have different observations on behaviour of process parameters on output quality characteristics of FSSW welds. It was observed that tensile-shear load (TSL) considerably varied with change in tool rotation speed, plunge depth, plunge rate, dwell time, tool profile and its dimensions etc. Suryanarayan and Sridhar [3] during investigations on FSSW of aluminium 6061observed bell-shaped behaviour of tensile shear load w.r.t tool rotations speed and shoulder diameter. With increase in rotational speed of tool and shoulder dimension, frictional heating increases which led to sufficient heat input and material flow and causes increased weld strength. With further increase in parameters, although increase in heat input was observed but it causes change in grain structure and accordingly

reduction in weld strength. Bozzi et al. [4] and Tozaki et al. [5] also had similar observation w.r.t rotational speed of tool for tensile-shear strength. On the contrary, behaviour of FSSW joints of Aluminium alloy of 5000 series with 6000 series showed an exponential increase in tensile shear load with rotation speed of tool [6]. It was because of increase in ductility of weld joint with increase in tool rotation speed, thereby increasing tensile-shear load. Rana et al. [7] attempted FSSW on a multi-layered aluminum polyethylene workpiece and observed increase and subsequently decrease in weld strength with increase in dwell time. This was attributed due to increased heat input and coarsening of grains at higher dwell time [8, 9]. Memon et al. [10] made an observation on influence of plunge depth on weld strength and stated that increased shoulder plunge depth results increased tensile-shear strength. This was due to improved mixing of materials and metallurgical bonding due to increased forging action of tool shoulder [11].

Literature reveals that sincere attempts were made by researchers to enhance the weld strength by changing process parameters. Therefore, there is need to design and develop a modified process to further enhance the weld characteristics. One method to achieve this is to obtain a metal matrix composite (MMC) at welding zone with the help of incorporation of ceramic reinforcement. The extraordinary properties of ceramic reinforcement such as high strength and melting point, low thermal expansion coefficient etc. certainly increase the weld strength [12–13]. Mishra et al. [14] fabricated a MMC on surface of aluminium alloy using Friction Stir Processing (FSP). They observed that silicon carbide (SiC) particles were homogeneously distributed within aluminum matrix, leading to excellent bond between reinforcements and matrix. After that, the idea was used to improve FSSW welds. The purpose of adding reinforcements was to enhance quality characteristics of welded joints with exclusive properties of ceramic reinforcement [15]. For instance, SiC has low thermal expansion coefficient, high melting point and high chemical and thermal stability. These properties of SiC helps in excellent coherence with matrix and reduces the chances of cracking.

Friction Stir Welding and Friction Stir Processing of different aluminium alloy with incorporation of various reinforcements like SiC [16], B_4C [17], TiB_2 [18] and Al_2O_3 [19] to modify and improve different properties of materials such as tribological etc. were reported in literature. Wu et al [20] obtained FSSW welds of AZ31 magnesium alloy with addition of reinforcements in stirring zone and stated that both microhardness and mechanical strength of welds were enhanced because of grain boundary strengthening. Tebyani and Dehghani [21] studies the effect of SiC particles on mechanical and microstructural properties of interstitial steel. Addition of SiC enhanced the quality of FSSW welds both in terms of mechanical strength and microhardness. They observed a decrease in grain size and stir zone, which therefore resulted in higher fracture load and microhardness [22].

In view of the above-mentioned literature, the objective of present work was to expand the existing understanding of effect of process parameters of welding, especially, incorporation of SiC particles in welds, on both microstructural and mechanical properties of FSSW welds. The present paper presents a detailed explanation of effect of SiC particles on quality characteristics of FSSW weld, such as tensile-shear strength, hook formation and weld structure.

2. Materials And Methods

Commercial grade aluminium 6061-T6 was used as workpiece material. The samples of size 120 mm × 30 mm × 3 mm were cut using diamond cutter. The positioning for spot weld was arranged using specially designed fixture with overlap area of 30 × 30 mm^2 as shown in Fig. 2. Silicon carbide (SiC) powder of 45 µm average particle size was used as reinforcement in the stirring zone. Reinforcement was placed in designed guide holes before start of plunging stage. The quantity of reinforcement was varied by changing dimensions of guiding hole and accordingly guiding holes of size 2.5, 3.0 and 3.5 mm were used. Apart from reinforcement quantity, tool rotational speed, pre-dwell time, dwell time, plunge rate, plunge depth considered as process parameters and their levels are presented in Table 1.

Table 1
Process Parameters

Sr. No.	Process Parameters	Level 1	Level 2	Level 3	Level 4
1.	Guiding Hole Diameter (mm)	0 (A_1)	2.5 (A_2)	3.0 (A_3)	3.5 (A_4)
2.	Tool Rotation Speed (rpm)	900 (B_1)	1300 (B_2)	1700 (B_3)	2100 (B_4)
3.	Pre-Dwelling Time (sec)	2 (C_1)	6 (C_2)	10 (C_3)	14 (C_4)
4.	Dwell Time (sec)	20	20	20	20
5.	Plunge Rate (mm/min)	15	15	15	15
6.	Plunge Depth (mm)	4.8	4.8	4.8	4.8

A computer numerical controlled (CNC) Vertical Machining Center (MAXMILL PLUS$^+$) available at Siemens Center of Excellence in Manufacturing was used to perform joining operation. The detailed experimental setup along with CNC Machining Center, joining tool, specially designed fixture to clamp workpieces is shown in Fig. 3. Specially designed joining tools used for experimentation were made from high carbon high chromium steel with average hardness of HRC 58. The joining tool had a zero concave angle shoulder and 4.8 mm long grooved pin. The tool shoulder diameter (D) of 16 mm, tool pin diameter (d) of 5mm and square pin tool profile was used for experimentations as shown in Fig. 4. The output quality characteristic of this experimentation was tensile-shear load and calculated using Universal Testing Machine (UTM), model number, UTE 40 HGFL. The test samples were mounted firmly on UTM, and progressive loading was applied till welded joint fractures. The accuracy of fractured load measured was ascertained by repeating the experiments three times. To explore macro and microstructural behaviour of welded joint, different tools and techniques were used such as stereo-zoom microscope (Stemi 508), Scanning Electron Microscope (SEM), Optical Microscopy (OM), Energy Dispersive Spectroscopy (EDS) etc. The sample preparation was considered as most important part for macro and microstructural behaviour which included polishing with emery papers of different grit sizes followed by polishing with alumina, brasso and velvet cloth to obtain a scratch free surface.

3. Results And Discussions

This section highlights general findings observed with tensile-shear testing of FSSW samples. The detailed mechanism for tensile-shear testing of FSSW joints produced at various process parameters and examination of their weld structure is provided in subsections below.

3.1 Weld Structure Examination:

During FSSW, workpiece material experiences plastic deformation. In case of reinforced FSSW weld, distribution of reinforced particles in welded region altered the weld properties at micro as well as macro structural level. The flow of material during FSSW process is a complex phenomenon and with addition of reinforcement further increases its complications. Cross-sectional macrograph of FSSW welded specimen obtained at 900 rpm of tool rotation speed, 6 sec of pre-dwelling time and 3.0 mm of guiding hole diameter, is shown in Fig. 5, and it was observed that the structure of weld was not symmetrical about weld centre. There were three regions identified at joining inter-face as Unbonded Region (UBR), Bonded Region (BR) and Partly Bonded Region (PBR). The left side of keyhole in which all three regions were observed is as shown in Fig. 5 (a). Bonding region was formed due to proper stirring and mixing of workpieces, resulting in merging of interfaces. During FSSW tool plunging, tool pushed the workpiece material down and deformed it while stirring. The process of stirring and deforming caused flow of material around pin in spiral form and transport material upward. This process caused mixing of two interfaces around pin and created region known as bonded region. After this region, effect of process parameters and heat generated reduced and incomplete material flow caused partial bonding of interfaces. Partially bonded region generally started with a void and then partial diffusion of interfaces took place due to incomplete material flow. After partially bonded region, a space between both interfaces was observed, known as unbonded region. The partially bonded region bent upward due to plunging action known as hook. Therefore, hook is generally a partially bonded region, bent in a radius like a mountain [23]. The void defects were also obtained on either side of keyhole due to improper flow of material and stirring zone was also small. While, cross-sectional view of rest of the sample showed presence of perfectly bonded regions, visually looking good and defect free. The amount of heat input plasticized the material and its flow played a vital role in obtaining defect-free weld [24]. The bonding region of leading (left) side was different from trailing (right) side. The width of bonding region on leading side of keyhole was 731.885 micron as shown in Fig. 5 (b) while on trailing side of keyhole bonding region of width 1005.932 micron was observed. A hook formation starting from the right side with a void was also observed. Although, bonded region was less in this sample but sufficient improvement in weld strength was observed due to incorporation of reinforcements.

The macrograph, optical microscopy and SEM images along with EDS analysis of weld at 3.0 mm guiding hole diameter, 1700 rpm tool rotation speed and 6 sec pre-dwelling time is as shown in Fig. 6. A clear interface between stirring zone and thermo-mechanically affected zone was observed, as shown in Fig. 6 (b) and (c). SEM image of stirring zone of FSSW weld confirms homogeneous distribution of SiC particles in stirring zone which is clearly visible in Fig. 6 (e-f). It is apparent from these micrographs, that

there was excellent bonding between reinforcement and matrix. Fig. 6 (g) shows the Electro Dispersive Spectroscopy (EDS) of FSSW weld and validates the presence of SiC particles in stirring zone of FSSW weld. The homogeneous distribution of SiC particles affect weld strength, because it restricts grain growth and act as hindrance for cracks to propagate easily. When tensile-shear load applied, it causes accumulation of plastic stress in region near to particle. When distance between particles is less, i.e., particles are homogeneously and closely placed, plastic flow of matrix gets trapped between reinforcements. The movement of dislocations restricted by particles, leads to increase in flow strength after yielding. When applied load exceeds critical value, stress releases and transferred to other particles. Therefore, the ductility and fracture load of the weld increases [25].

Whereas, Fig.7, shows SEM image of sample obtained at 1300 rpm, 6 sec pre-dwelling time and 3.5 mm guiding hole diameter, in which clusters of SiC particles were observed. This clustering was due to improper material flow and mixing of reinforcements. A cluster was considered as one single big particle, leading to inhomogeneity due to random placement of these particles. Therefore, distance between particles increases. When load is applied, large particles act as nucleation sites, which initiates stress and strain fields and helps in easy breaking of matrix-reinforcement interface. After, damaging interface, released stress fields moves fast to other particles placed at far distance without any significant disturbances and causes decrease in fracture load of weld. Therefore, clustered reinforcements are regarded as the site of initiation of premature failure [26]. The clustering can be avoided by choosing appropriate process parameters to increase heat input for inducing sufficient material flow and mixing of reinforcement in stirring zone. Hence, homogeneous distribution of SiC particles plays an important role in strengthening of the welded joint. The homogeneity of reinforcements was visible in most of the welds, studied in the research investigation.

3.2 Effect of process parameters on Tensile-Shear Load of FSSW weld:

Pictorial representation of tensile-shear testing of FSSW samples is shown in Fig. 8. After experimentation, FSSW welds were prepared for tensile-shear testing. The specimens were made equiaxed by adhering two aluminium pieces of same thickness at edges of workpieces to make weld sample aligned before mounting on UTM followed by gradually increasing tensile-shear load. The behaviour of tensile-shear load with variation in guiding hole diameter i.e., quantity of SiC particles, tool rotation speed and pre-dwelling time is presented in Fig. 9, Fig. 13 and Fig. 15 respectively.

The bahaviour of tensile-shear load with variation in guiding hole diameter i.e., quantity of SiC particles is presented in Fig. 9. It was observed that tensile-shear load significantly increased with increase in guiding hole diameter. The tensile shear load of FSSW weld produced without SiC particles was compared with welds produced with different quantities of SiC particles present in stirring zone, i.e., 25% (2.5 mm diameter), 36% (3.0 mm diameter) and 49% (3.5 mm diameter) of volume fraction. The maximum weld strength of 4952.07 N was obtained in sample produced with 49% volume fraction SiC particles, which was 29.78% higher than weld produced without SiC particles. When rotating tool plunges in workpiece

material, SiC particles blend with workpiece material in stirring zone and surrounded the aluminium grains, which causes increased weld strength. This improvement in weld strength was because of reinforced SiC particles having superior mechanical and thermal properties which helps in reducing grain growth occurred due to increased heat input and causes dynamic recrystallization of aluminium grains. However, SiC particles, surrounding aluminium grains, resists grain growth as SiC particles do not expand with increasing heat input, known as Zenner pinning effect, shown in Fig. 10. It can be noted from Fig. 10 that grain boundaries are pinned by reinforcements present around them and their growth is restricted. Thus, refined microstructure was obtained which led to increased tensile-shear strength. While, grain boundaries without reinforcements grow freely and comparatively coarser grains are obtained.

Another possible reason for increase in tensile-shear strength with SiC particles is difference in thermal expansion coefficient of aluminium alloy and SiC particles. When FSSW joints cool down, strain fields formed around SiC particles, leading to formation of dislocations [27]. When FSSW weld subjected to tensile-shear loading, strain fields increase, which leads to piling up of dislocations and these piled up dislocations act as barrier on the way of crack propagation. Therefore, tensile-shear load increases as higher load required to break through piled-up dislocations and SiC particles. Apart from this, SiC particles act as shield that holds the applied forces and does not allow to damage aluminium grains and acts as hindrance for cracks to propagate, shown in Fig. 11. [28]. This continues until force becomes large enough to damage aluminium-SiC interface. It can be concluded that fracture of the joint starts with tearing of aluminium-SiC particles interface then propagate in weld region. However, as number of SiC particles increase, strain and stress field decrease as load is distributed to large number of particles and number of dislocations are blocked. This process limits the plastic zone around SiC particles and when this strain and stress fields increases to a critical value, fracture of particles take place [29].

In addition, a significant increase in strength of SiC-reinforced weld is associated with simultaneous increase in the elongation of the weld when subjected to tensile-shear load. Load-displacement curve of welds at varied reinforcement quantity is shown in Fig. 12. It is clear from Fig. 12 that, sample with reinforcements has elongated more as compared to sample without reinforcements due to grain refinement. As size of grains decreases, ductility of weld increases, which results in higher displacement obtained at higher tensile-shear load. All these factors aid in increasing strength of FSSW welds and shows dominating positive effect of SiC in improving tensile-shear load of the welds.

On the contrary, it was observed from Fig. 13 that tensile-shear load increased with increase in tool rotation speed and then decreased. As tool rotation speed increased from 900 rpm (B_1) to 1700 rpm (B_3), tensile-shear load is increased from 4110.51 N to 4600.22 N. Whereas, the further increase in tool rotation speed to 2100 rpm (B_4), tensile-shear load decreased to 4498.17 N. The apparent reason for this can be explained in terms of elongation, shown in load versus displacement curve (Fig. 14). The elongation of weld first increased from B_1 to B_3, then reduced at B_4. With decrease in size of grains greater number of grain boundaries were obtained and higher load was required to break through these boundaries. This increases ductility of weld, hence increases strength of weld. However, the phenomenon of obtaining smaller or larger grains depends on amount of heat input. With increase in rotational speed of tool,

temperature and heat input to the workpiece increases and softens the workpiece which assist in easy material flow and mixing. During this process, refinement of grains in stir zone (SZ) takes place. Therefore, refined microstructure was obtained in SZ, which increase fracture load of joint. However, higher tool rotation speed led to higher heat input, which means weld will take more time to cool down. The slower cooling rate of weld gives more time to grains for dynamic recrystallisation, i.e., coarsening of grains due to grain growth. Therefore, fracture load of weld decreases. The strain rate also plays an important role for grain refinement with increased tool rotation speed. When rotational speed of tool increases up to 1700 rpm, strain rate increases, which has positive effect on weld strength. The increase in strain rate restricts the motion of dislocations which get activated due to mechanical and thermal activities [30]. However, with additional increase in rotational speed of tool, influence of strain rate was overpowered by heat input and its effect on grain modification and ultimately weld strength. This behaviour of tool rotation speed is similar to previous researches on influence of rotation speed of tool on weld strength [23].

The behaviour of tensile-shear load with pre-dwelling time at constant guiding hole diameter (3.0 mm) and tool rotation speed (1300 rpm) is shown in Fig. 15. Tensile-shear load dominantly increased with increase in pre-dwelling time. The increase in pre-dwelling time from 2 sec (C_1) to 14 sec (C_4) increased weld strength from 4191.51 N to 4544.02 N. This was because when pre-dwelling time increased, the tool came in contact with upper workpiece for more time, which increased frictional heat input. The upper workpiece material became soft and helped in easy plunging of tool and developed required material flow. Hence, adequate material flow and mixing of both workpiece material led to proper bonding of both workpieces. The increase in bonding of weld lead to increased elongation of weld when load was applied, shown in Fig. 16. Hence, higher tensile-shear load was required to break the weld. However, pre-dwelling time also has a positive effect on tool because when workpiece becomes softer with higher pre-dwelling time, tool can easily plunge into the workpiece without facing any sudden impact. Also, when tool plunges easily into workpiece, the microstructure of workpiece not altered significantly. Therefore, higher pre-dwelling time is preferable for obtaining sound welds. Researchers have used different methods and equipment to pre-heat the specimen such as butane torch [31], induction coil [32], resistance rod [33] etc. and observed improved weld strength after pre heating the upper workpiece. Same observations were obtained in present study when pre-heating was done using friction between workpiece and tool. However, the method employed for pre-heating in present work didn’t require any special equipment, making the process economically beneficial.

From aforementioned facts and experimental observations, it can be concluded that welds attained at lower tool rotation speed and pre-dwelling time were not strong enough as compared to other welds. The reason behind this can be the formation of insufficient bonding between two workpieces. When both tool rotation speed and pre-dwelling time were low the heat produced was not sufficient to form a good welded joint. As shown in Fig. 9, Fig. 13 and Fig. 15, maximum strength was obtained at 3.5 mm of guiding hole diameter, tool rotation speed of 1700 rpm and pre-dwelling time of 14 secs. Hence, it can be

concluded that maximum weld strength can be obtained at combination of higher quantity of reinforcement and pre-dwelling time and intermediary tool rotation speed.

4. Conclusion

In this study, FSSW welds of Al 6061-T6 were produced with incorporation of SiC particles in the weld region. Influence of SiC particles on mechanical properties and weld structure was analysed and discussed. The attained results during this study are summarized as follows:

- Weld structure examination of FSSW welds revealed homogeneous distribution of SiC particles in stirring zone.
- A good coherence between SiC particles and aluminium matrix was observed from SEM images. The EDS analysis confirmed presence of SiC particles in stirring zone.
- The tensile-shear load of FSSW welds increased with increasing guiding hole diameter. FSSW weld obtained at 3.5 mm guiding hole diameter showed an increase of 29.78% in comparison with weld obtained without incorporation of reinforcements.
- Guiding hole diameter was observed as significant parameter for improved weld strength.
- Welds obtained at varied tool rotation speed, showed enhancement in weld strength up-to 1700 rpm and then a decrease at 2100 rpm.
- An increasing trend of tensile-shear load w.r.t to pre-dwelling time was observed with increasing pre-dwelling time.
- The method used in present research for pre-heating the workpiece was found to be economical as there was no special equipment used to serve the purpose.
- Higher values of guiding hole diameter as well as pre-dwelling time and moderate value of tool rotation speed was considered as a good combination of process parameters for obtaining optimum FSSW welds.

Declarations

Acknowledgement

The authors wish to acknowledge SIEMENS Centre of Excellence, Punjab Engineering College (Deemed to be University), Chandigarh for providing research facility.

Declaration

The authors declare that no funds or grants were received during this research investigation and both authors have read and approved the final manuscript.

References

1. Enami, M., Farahani, M., & Farhang, M. (2019). Novel study on keyhole less friction stir spot welding of Al 2024 reinforced with alumina nanopowder. The International Journal of Advanced Manufacturing Technology, 101(9), 3093-3106.
2. R.S. Mishra, Z.Y. Ma, Friction stir welding and processing, Mater. Sci. Eng. R 50 (2005) 1–78.
3. Suryanarayanan, R., & Sridhar, V. G. (2020). Effect of Process Parameters in Pinless Friction Stir Spot Welding of Al 5754-Al 6061 Alloys. *Metallography, Microstructure, and Analysis*, *9*(2), 261-272.
4. Bozzi, S., Helbert-Etter, A. L., Baudin, T., Klosek, V., Kerbiguet, J. G., & Criqui, B. (2010). Influence of FSSW parameters on fracture mechanisms of 5182 aluminium welds. *Journal of Materials Processing Technology*, *210*(11), 1429-1435.
5. Tozaki, Y., Uematsu, Y., & Tokaji, K. (2008). Effect of tool shoulder diameter on mechanical properties of friction stir spot welded joints. *Trans. Jpn. Soc. Mech. Eng. A*, *74*, 268-274.
6. Patel, V. V., Sejani, D. J., Patel, N. J., Vora, J. J., Gadhvi, B. J., Padodara, N. R., & Vamja, C. D. (2016). Effect of tool rotation speed on friction stir spot welded AA5052-H32 and AA6082-T6 dissimilar aluminum alloys. Metallography, Microstructure, and Analysis, 5(2), 142-148.
7. Rana, P. K., Narayanan, R. G., & Kailas, S. V. (2021). Assessing the dwell time effect during friction stir spot welding of aluminum polyethylene multilayer sheets by experiments and numerical simulations. *The International Journal of Advanced Manufacturing Technology*, 114(7), 1953-1973.
8. Li, G., Zhou, L., Zhou, W., Song, X., & Huang, Y. (2019). Influence of dwell time on microstructure evolution and mechanical properties of dissimilar friction stir spot welded aluminum–copper metals. *Journal of Materials Research and Technology*, 8(3), 2613-2624.
9. Fereiduni, E., Movahedi, M., Kokabi, A. H., & Najafı, H. (2017). Effect of dwell time on joint interface microstructure and strength of dissimilar friction stir spot-welded Al-5083 and St-12 alloy sheets. *Metallurgical and Materials Transactions* A, 48(4), 1744-1758.
10. Memon, S., Paidar, M., Mehta, K. P., Babaei, B., & Lankarani, H. M. (2021). Friction spot extrusion welding on dissimilar materials AA2024-T3 to AA5754-O: effect of shoulder plunge depth. *Journal of Materials Engineering and Performance*, *30*(1), 334-345.
11. Muhayat, N., Triyono, R. D. R., & Zubaydi, A. (2018). Effect of Tool Plunge Depth and Pin Profile on Mechanical Properties of Friction Stir Spot Welded AA5052 Joints. *Journal of Mechanical Engineering (JMechE)*, *15*(1), 181-191.
12. Sapuan, S. M., & Mujtaba, I. M. (Eds.). (2009). Composite materials technology: neural network applications. CRC Press.
13. Asadollahi, M., & Khalkhali, A. (2018). Optimization of mechanical and microstructural properties of friction stir spot welded AA 6061-T6 reinforced with SiC nanoparticles. *Materials Research Express*, 5(11), 116517.
14. Mishra, R. S., Mahoney, M. W., McFaden, S. X., Mara, N. A., & Mukherjee, A. K. (1999). High strain rate superplasticity in a friction stir processed 7075 Al alloy. *Scripta Materialia*, 42(2).
15. Arul, S. G. (2009). *Experimental analysis of spot friction welding of 6111-T4 aluminum alloy* (Doctoral dissertation, University of Michigan College of Engineering Graduate Professional

Programs).

16. Barmouz, M., Asadi, P., Givi, M. B., & Taherishargh, M. (2011). Investigation of mechanical properties of Cu/SiC composite fabricated by FSP: Effect of SiC particles' size and volume fraction. *Materials Science and Engineering: A*, *528*(3), 1740-1749.
17. Paidar, M., Ojo, O. O., Ezatpour, H. R., & Heidarzadeh, A. (2019). Influence of multi-pass FSP on the microstructure, mechanical properties and tribological characterization of Al/B4C composite fabricated by accumulative roll bonding (ARB). *Surface and Coatings Technology*, *361*, 159-169.
18. Sethi, D., Kumar, S., Shekhar, S., & Roy, B. S. (2021). Friction stir welding of AA7075-T6/TiB2 in situ cast composites plates using scarf joint configuration. *Advances in Materials and Processing Technologies*, 1-13.
19. Jamalian, H. M., Eskandar, M. T., Chamanara, A., Karimzadeh, R., & Yousefian, R. (2021). An artificial neural network model for multi-pass tool pin varying FSW of AA5086-H34 plates reinforced with Al2O3 nanoparticles and optimization for tool design insight. *CIRP Journal of Manufacturing Science and Technology*, *35*, 69-79.
20. Wu, D., Shen, J., Lv, L., Wen, L., & Xie, X. (2017). Effects of nano-SiC particles on the FSSW welded AZ31 magnesium alloy joints. *Materials Science and Technology*, 33(8), 998-1003.
21. Tebyani, S. F., & Dehghani, K. (2016). Effects of SiC nanopowders on the mechanical properties and microstructure of interstitial free steel joined via friction stir spot welding. *Materials & Design*, 90, 660-668.
22. Suresh, S., Elango, N., Venkatesan, K., Lim, W. H., Palanikumar, K., & Rajesh, S. (2020). Sustainable friction stir spot welding of 6061-T6 aluminium alloy using improved non-dominated sorting teaching learning algorithm. *Journal of Materials Research and Technology*, 9(5), 11650-11674.
23. Shen, Z., Yang, X., Zhang, Z., Cui, L., & Yin, Y. (2013). Mechanical properties and failure mechanisms of friction stir spot welds of AA 6061-T4 sheets. *Materials & Design*, 49, 181.
24. Lambiase, F., Paoletti, A., & Di Ilio, A. (2015). Mechanical behaviour of friction stir spot welds of polycarbonate sheets. *The International Journal of Advanced Manufacturing Technology*, 80(1), 301-314.
25. Prabu, S. B., & Karunamoorthy, L. (2008). Microstructure-based finite element analysis of failure prediction in particle-reinforced metal–matrix composite*. journal of materials processing technology*, 207(1-3), 53-62.
26. Azizieh, M., Kokabi, A. H., & Abachi, P. (2011). Effect of rotational speed and probe profile on microstructure and hardness of AZ31/Al2O3 nanocomposites fabricated by friction stir processing. *Materials & Design*, 32(4), 2034-2041.
27. Jeong, Y. H., Hong, S. T., Hasan, M. T., Tien, H. N., Hur, S. H., & Kwon, Y. J. (2014). Mechanical properties of graphite/aluminum metal matrix composite joints by friction stir spot welding. *Journal of Mechanical Science and Technology*, 28(2), 499-504.
28. Doel, T. J. A., & Bowen, P. (1996). Tensile properties of particulate-reinforced metal matrix composites. *Composites Part A: Applied Science and Manufacturing*, 27(8), 655-665.

29. Sozhamannan, G. G., Prabu, S. B., & Paskaramoorthy, R. (2010). Failures analysis of particle reinforced metal matrix composites by microstructure based models. *Materials & Design*, 31(8), 3785-3790.
30. Wang, W., Ma, Y., Yang, M., Jiang, P., Yuan, F., & Wu, X. (2018). Strain rate effect on tensile behavior for a high specific strength steel: From quasi-static to intermediate strain rates. *Metals*, 8(1), 11.
31. Garg, A., & Bhattacharya, A. (2020). Friction stir spot welding of AA6061-T6 and Cu with preheating: strength and failure behavior at different test temperatures. *The International Journal of Advanced Manufacturing Technology*, 108, 1613-1629.
32. Sun, Y. F., Shen, J. M., Morisada, Y., & Fujii, H. (2014). Spot friction stir welding of low carbon steel plates preheated by high frequency induction. *Materials & Design* (1980-2015), 54, 450-457.
33. Shen, J., Min, D., & Wang, D. (2011). Effects of heating process on the microstructures and tensile properties of friction stir spot welded AZ31 magnesium alloy plates. *Materials & Design*, 32(10), 5033-5037.

Figures

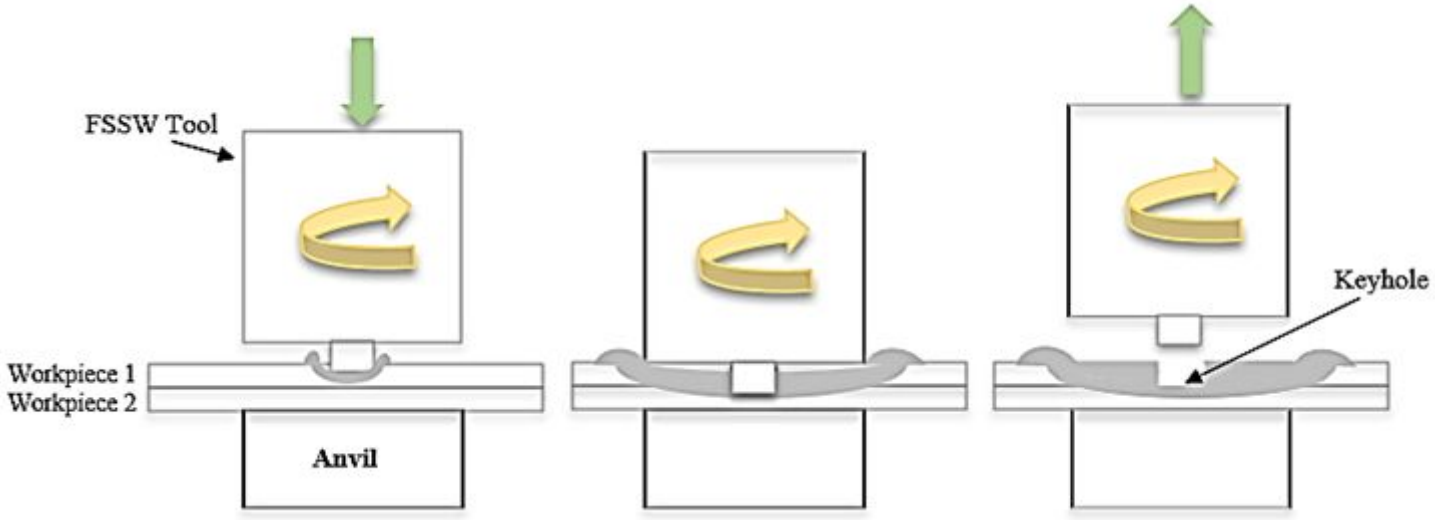

Figure 1

Schematic of FSSW process: (a) Plunging, (b) Stirring and (c) Retracting

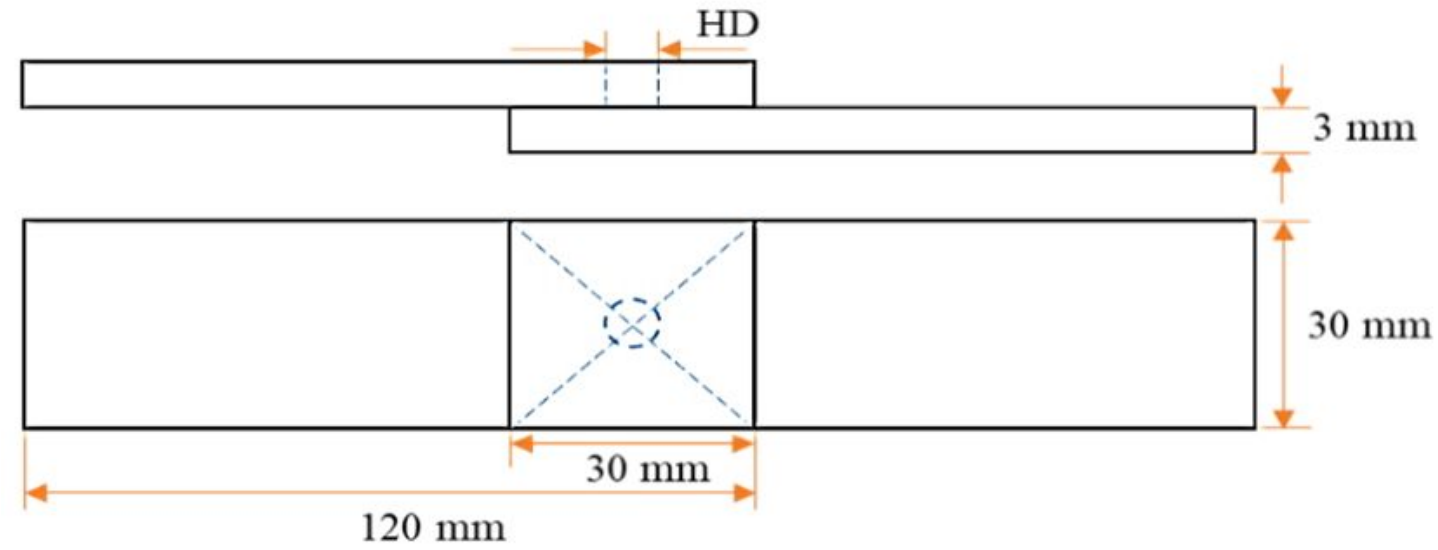

Figure 2

Test Specimen Configuration

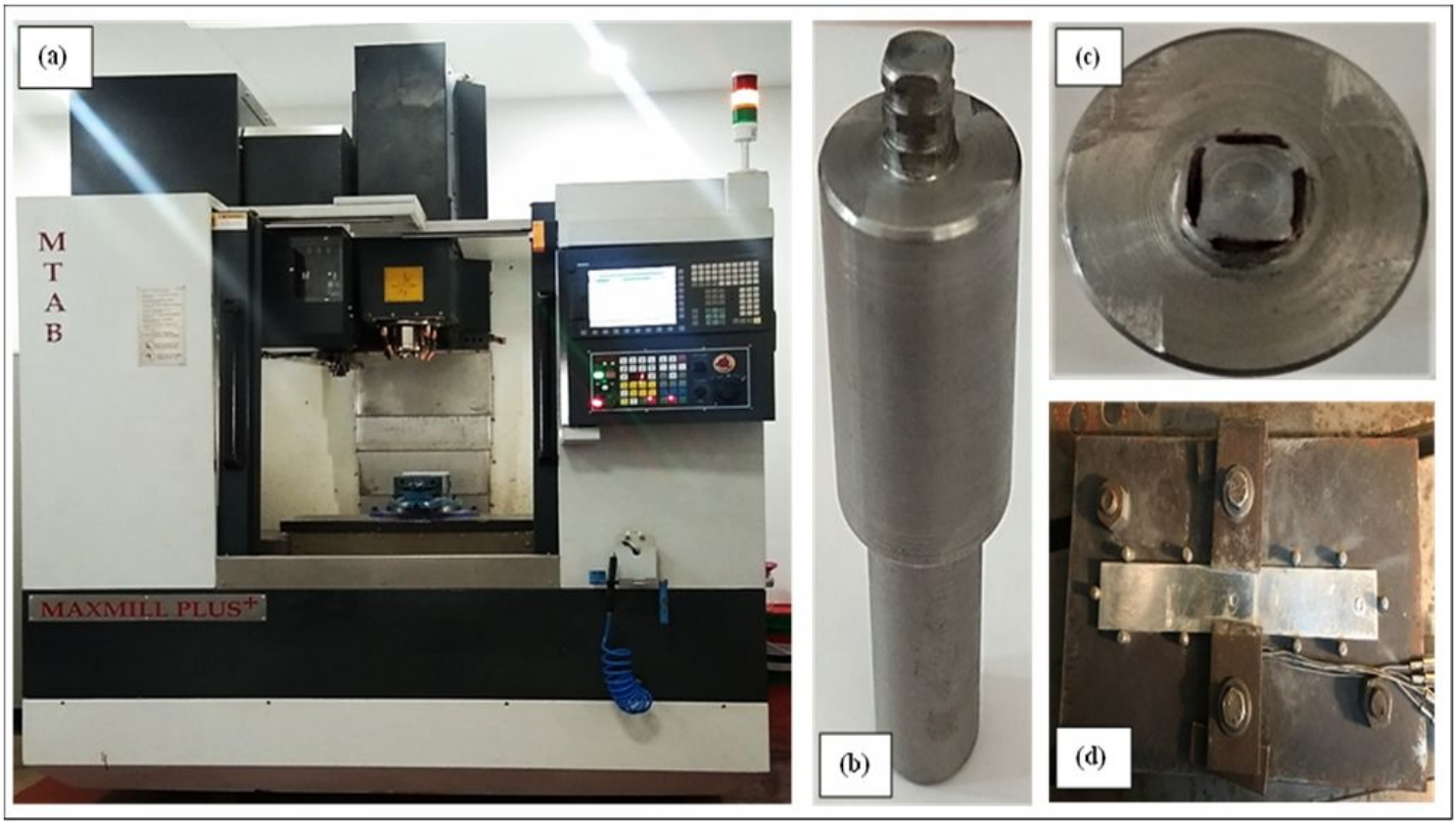

Figure 3

Experimental Setup (a) CNC Milling Machine, (b & c) FSSW Tool and (d) Fixture

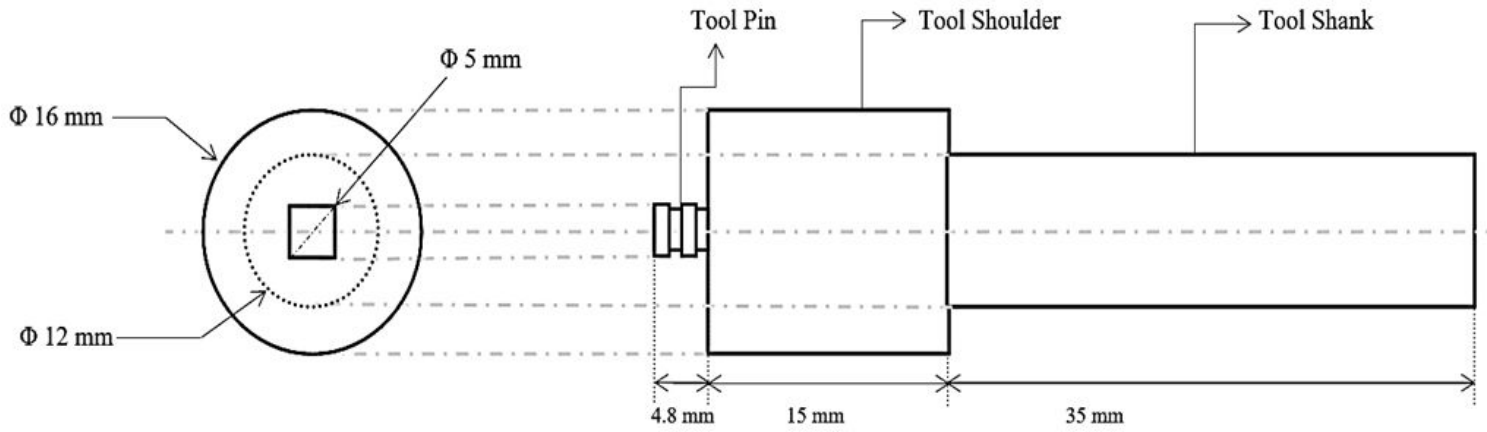

Figure 4

FSSW Tool Dimensions

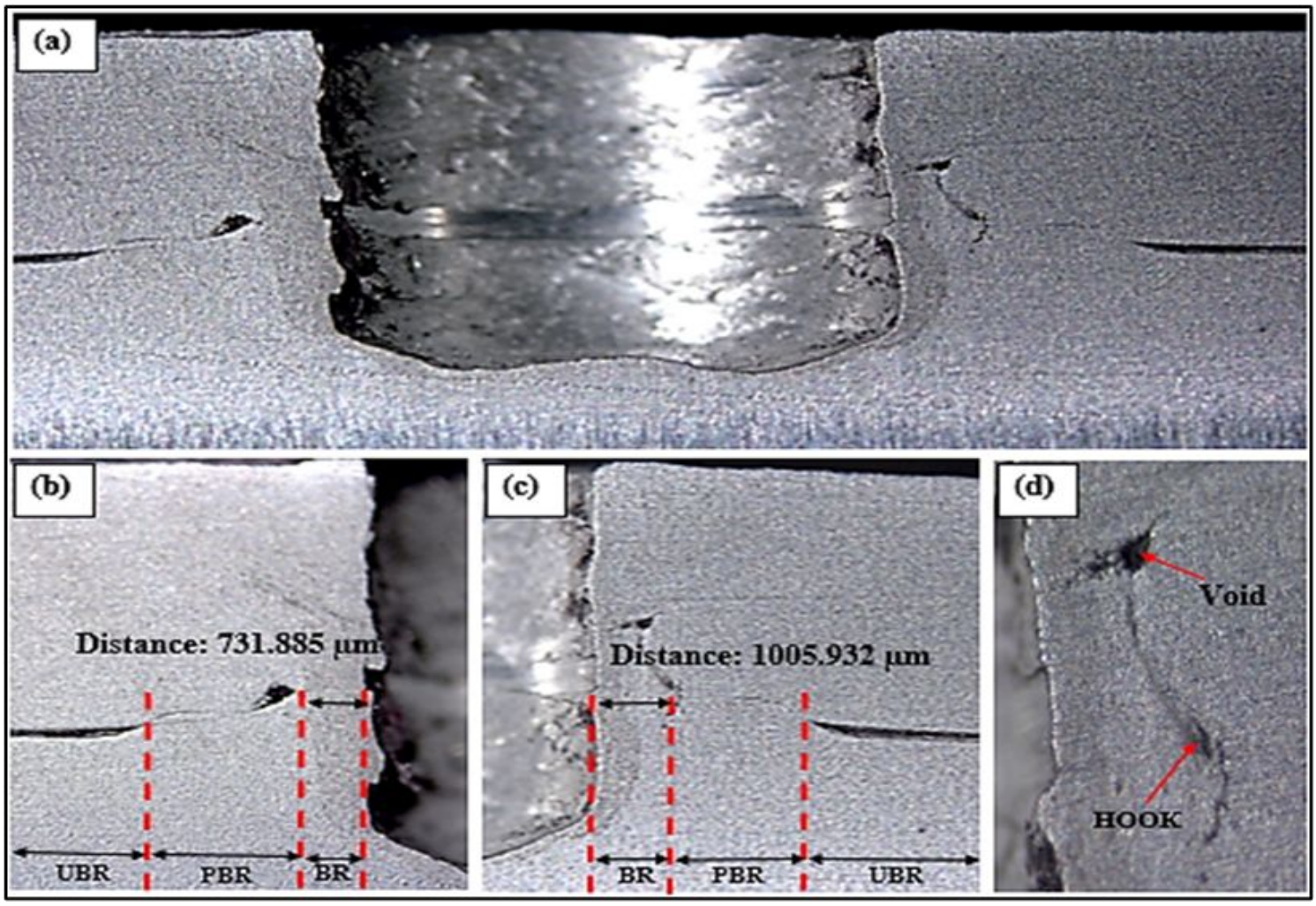

Figure 5

(a) Macrograph of sample obtained at 900 rpm Tool Rotation Speed, 6 sec Pre-Dwelling time and 3.0 mm Guiding Hole Diameter, (b) Macrograph of left-side of keyhole, (b) Macrograph of right-side of keyhole

and (d) Hook

Figure 6

(a) Macrograph of cross-section of FSSW weld with produced at 1700 rpm Tool Rotation Speed, 6 secs Pre-dwelling Time and 3.0 mm Guiding Hole Diameter (b), (c) different regions of cross-sections and (d) Uniformly distributed SiC particles. (e) SEM image of SZ at 10 μm, (f) SEM image of SZ at 5 μm and (g) EDS profile of particle present in SZ

Figure 7

(a) Macrograph of FSSW weld obtained at 1300 rpm Tool Rotation Speed, 6 secs Pre-dwelling Time and 3.5 mm Guiding Hole Diameter, (b) SEM image of SZ at 10 μm and (c) EDS profile of particle present in SZ

Figure 8

(a) FSSW samples, (b) FSSW Tensile-Shear Testing Sample, (c) FSSW Testing Sample held in UTM and (d) Fractured sample.

Figure 9

Effect of guiding hole diameter on tensile-shear load at tool rotation speed of 1300 rpm and 6 secs of pre-dwelling time

Figure 10

Zenner Pinning Effect

Figure 11

Crack propagation through reinforced matrix

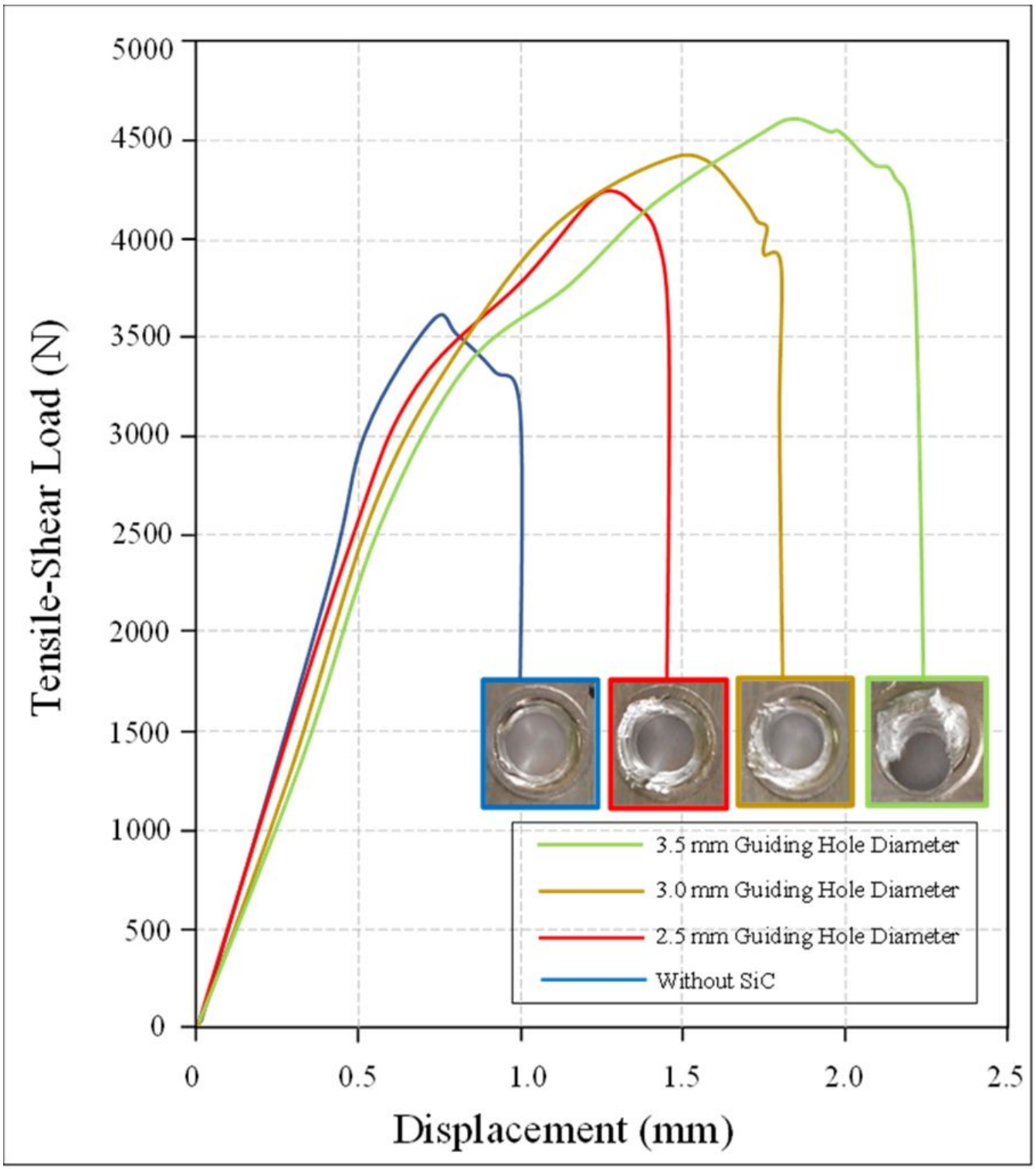

Figure 12

Load-Displacement Curve at different Guiding Hole Diameter, 1300 rpm tool rotation speed, 6 sec dwelling time and top view of bottom workpiece of fractured weld specimen

Figure 13

Effect of tool rotation speed on tensile-shear load at guiding hole diameter of 3.0 mm and 6 secs of pre-dwelling time

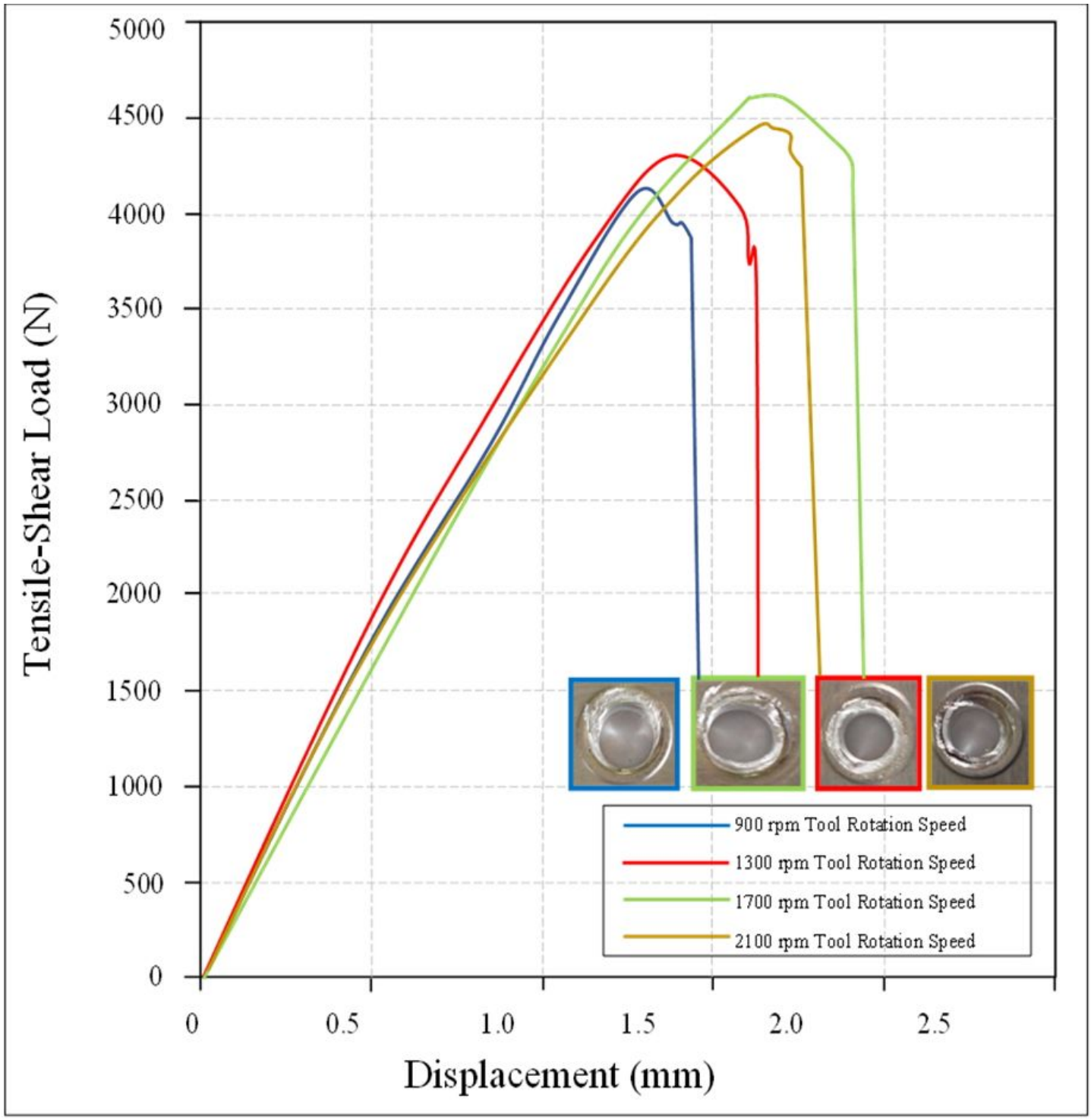

Figure 14

Load-Displacement Curve at different Tool Rotation Speed, 3.0 mm guiding hole diameter, 6 sec pre-dwelling time and top view of bottom workpiece of fractured weld specimen

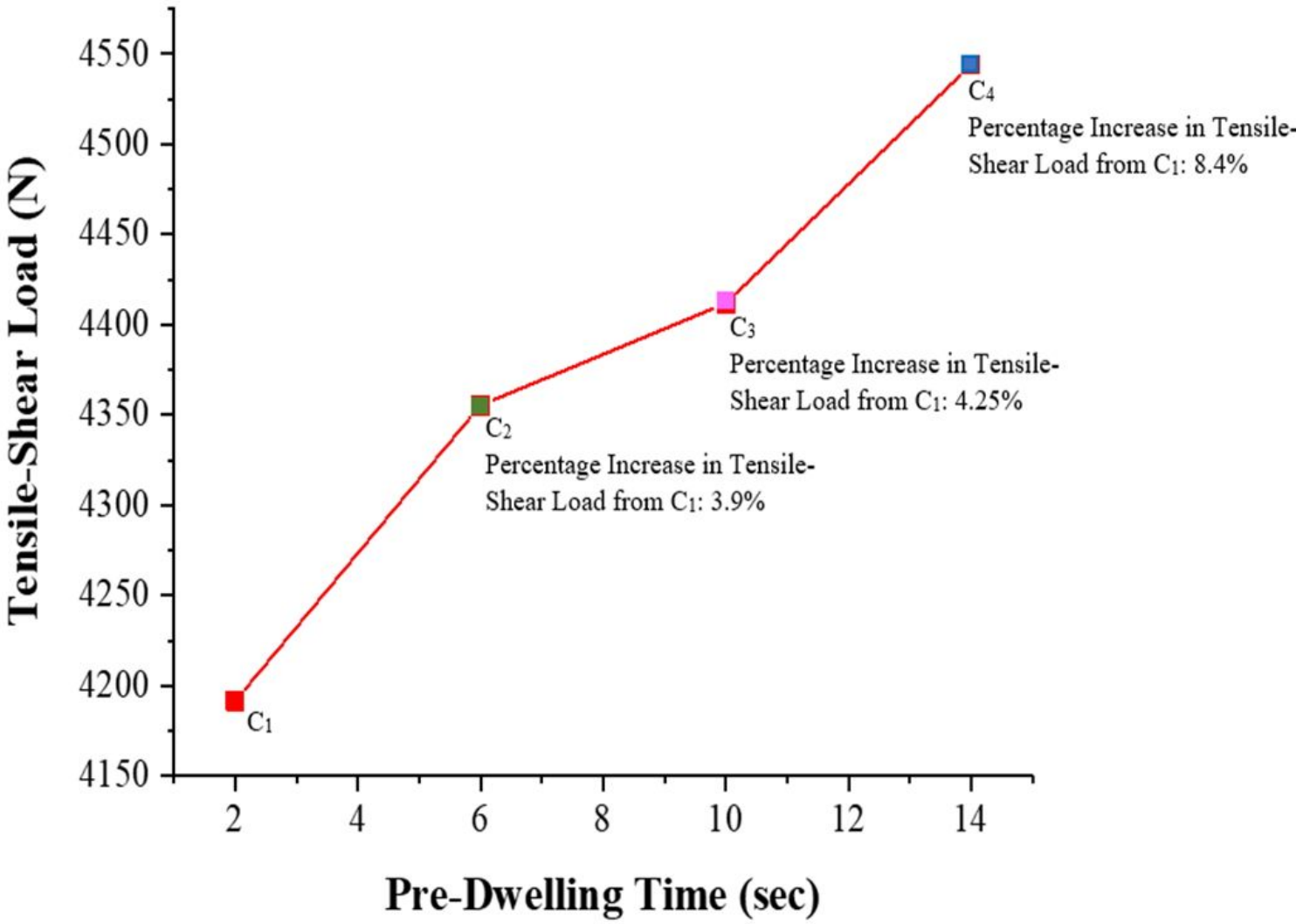

Figure 15

Effect of Pre-Dwelling Time on Tensile-Shear Load at Guiding Hole Diameter of 3.0 mm and 1300 rpm of Tool Rotation Time

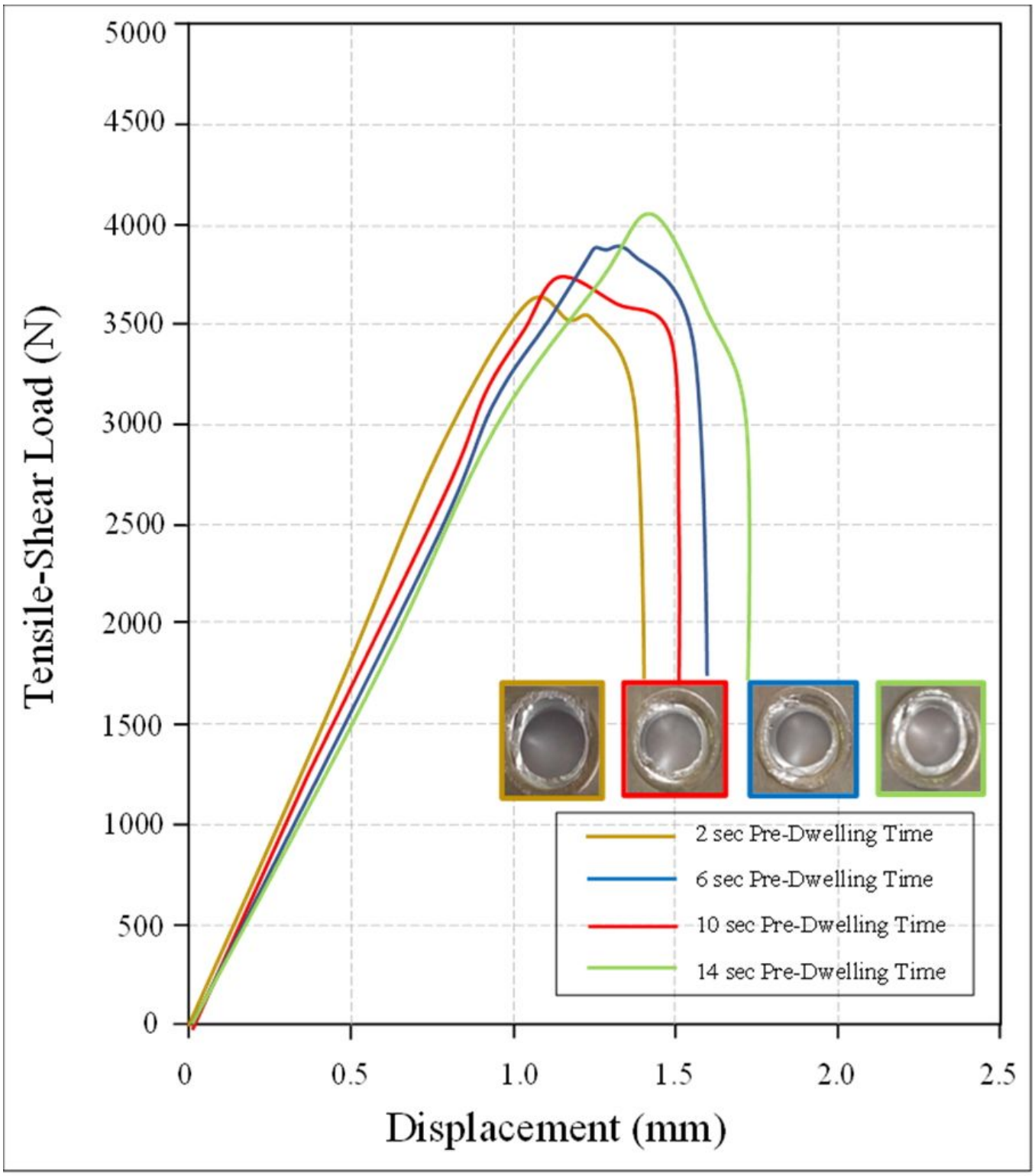

Figure 16

Load-Displacement Curve at different Pre-Dwelling Time, 1300 rpm tool rotation speed, 3.0 mm guiding hole diameter and top view of bottom workpiece of fractured weld specimen